Deon *et al. Geotherm Energy (2015) 3:20*
DOI 10.1186/s40517-015-0040-6

Geothermal Energy
a SpringerOpen Journal

RESEARCH Open Access

# Geochemical/hydrochemical evaluation of the geothermal potential of the Lamongan volcanic field (Eastern Java, Indonesia)

Fiorenza Deon[1*], Hans-Jürgen Förster[2], Maren Brehme[2], Bettina Wiegand[3], Traugott Scheytt[4], Inga Moeck[5], Makky S. Jaya[6] and Dewi J. Putriatni[7]

*Correspondence:
F.Deon@tudelft.nl
[1] Delft University of Technology, Department of Geoscience and Engineering, Delft, The Netherlands
Full list of author information is available at the end of the article

**Abstract**

Magmatic settings involving active volcanism are potential locations for economic geothermal systems due to the occurrence of high temperature and steam pressures. Indonesia, located along active plate margins, hosts more than 100 volcanoes and, therefore, belongs to the regions with the greatest geothermal potential worldwide. However, tropical conditions and steep terrain reduce the spectrum of applicable exploration methods, in particular in remote areas. In a case study from the Lamongan volcanic field in East Java, we combine field-based data on the regional structural geology, elemental and isotopic composition of thermal waters, and the mineralogical and geochemical signatures of volcanic rocks in exploring hidden geothermal systems. Results suggest infiltration of groundwater at the volcanoes and faults. After infiltration, water is heated and reacts with rocks before rising to the surface. The existence of a potential heat source is petrologically and geophysically constrained to be an active shallow mafic-magma chamber, but its occurrence is not properly reflected in the composition of the collected warmed spring waters that are predominantly meteoric in origin. In conclusion, spring temperature and hydrochemistry alone may not always correctly reflect the deep geothermal potential of an area.

**Keywords:** Geothermal exploration, Hidden magmatic systems, Rock petrology

## Background

In a conventional approach, several methods need to be adopted and integrated to understand the geochemical and geophysical signatures of active geothermal systems (e.g., Rybach and Muffler 1981). These methods also apply for greenfield studies and include: (a) geochemical investigations, e.g., application of chemical geothermometers to infer the temperature of the geothermal reservoir; measurement of gas isotopes, such as $^{3}He/^{4}He$, to constrain the origin (mantle or crust) of fluids; (b) drilling of exploration wells; (c) gravity measurements to map any negative anomaly associated with the steam fraction in high-porosity reservoir rocks or to locate zones of lowered density provoked by thermal expansion in magmatic bodies; (d) application of electrical methods such as resistivity to search for zones of higher-salinity fluids; (e) use of seismic methods for the localization of shallow intrusions and estimation of their vertical extension.

Young volcanic zones along convergent plate margins are prime targets for the exploration of geothermal energy sources, as active magma chambers have an intrinsically high geothermal potential (Bogie et al. 2005). Heat transfer in those areas is dominated by circulating fluids and, in the case of two-phase systems, also by steam. Therefore, surface manifestations, such as hot springs and steam vents, are indicators for geothermal activity. Prior to any geophysical surveying of geothermal systems, a field-based geological and geochemical reconnaissance is required to develop a conceptual model of a geothermal field. The exploration phase predating drilling of the first well is commonly termed greenfield exploration, referring to the juvenile non-exploited condition of a geothermal reservoir (Hochstein 1988). However, superficial geothermal manifestations are not manifested in all volcanic fields. Geological formations serving as barriers or seals for fluids may prevent discharge of up-flowing waters. Java is geologically associated with the magmatic arc of the Sunda subduction zone (Simkin and Siebert 1994). Here, geothermal waters were the subject of exploration and utilization over several decades (Hochstein and Browne 2000; Hochstein and Sudarman 2008). However, the efforts to explore and exploit geothermal prospects have changed over the years and also with respect to their location along the island chain. For example, activities for exploitation of geothermal energy centered on vapor-dominated systems in western and central Java (in Salak or Cisolok) at the end of the 1970s, where the infrastructure was sufficiently developed. Efforts increased in the mid-1990s, when the Indonesian government encouraged foreign investors to take part in the exploration. Recently, the main activities are focused on existing power plants at Kamojang, Wyang Windu and Djeng. The eastern part of Java, however, is still only poorly explored although several active magmatic fields like the Lamongan volcanic field (LVF) (Fig. 1), located southeast of Surabaya in eastern Java, are known to exist. Tropical conditions, steep terrain and difficult access could explain why a well-substantiated geothermal concept for East Java is still missing.

This study provides a first survey of the geothermal potential of the Tiris area located on the northeastern slope of Lamongan Volcano in East Java, Indonesia (Figs. 1, 2). It is assumed that the Tiris area hosts a geothermal system, as there are some surface geothermal manifestations (warm and hot springs) located along the Tancak River (Fig. 2). On the other hand, zeolite-bearing veins, for example, indicative of satellite boiling zones along the hydrothermal outflow zone and, therefore, also indicative of deep-seated geothermal reservoirs (e.g., Lawless et al. 1995), are absent at Tiris. The purpose of this study is to develop a conceptual model of the Tiris geothermal system in the Lamongan Volcanic Field (LVF) by combining field observations and chemical data of hot and warm springs with a reconnaissance structural–geological mapping, which will serve as a baseline study for a subsequent in-depth geological and seismic exploration of the area. The following methods were applied for the characterization and chemical and isotopic analyses of fluid and rock samples: electron microprobe analysis (EMPA), Inductively Coupled Plasma Atomic-Emission Spectrometry (ICP-AES), Atomic Absorption Spectrophotometry (AAS), X-ray diffraction (XRD), X-ray fluorescence (XRF), and mass-spectrometric determination of radioactive (Sr) and stable ($^{18}O$ and $^{2}H$) isotopes.

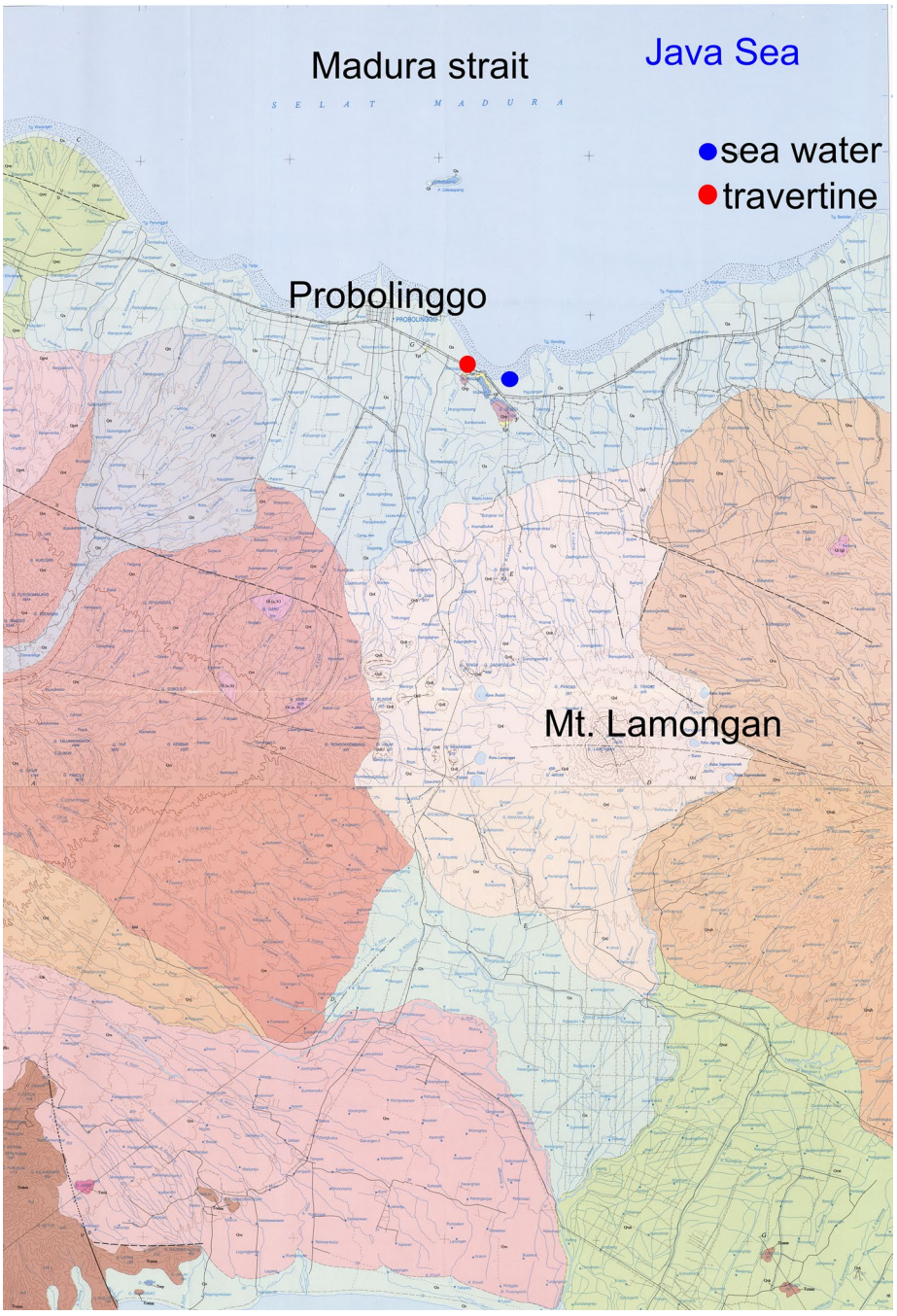


**Fig. 1** Geological map of the region Probolinggo Lumajang in Eastern Java Indonesia showing the location of this study investigation area (Mt. Lamongan)

## Geological setting

Gunung Lamongan (8.00°S, 113.342°E, and 1625 m above sea level) is one of several active volcanoes located in East Java. During the nineteenth century, Gunung Lamongan (last eruption in 1898) was among the most active volcanoes in Indonesia and seismic activity is ongoing since then (Carn 2000).

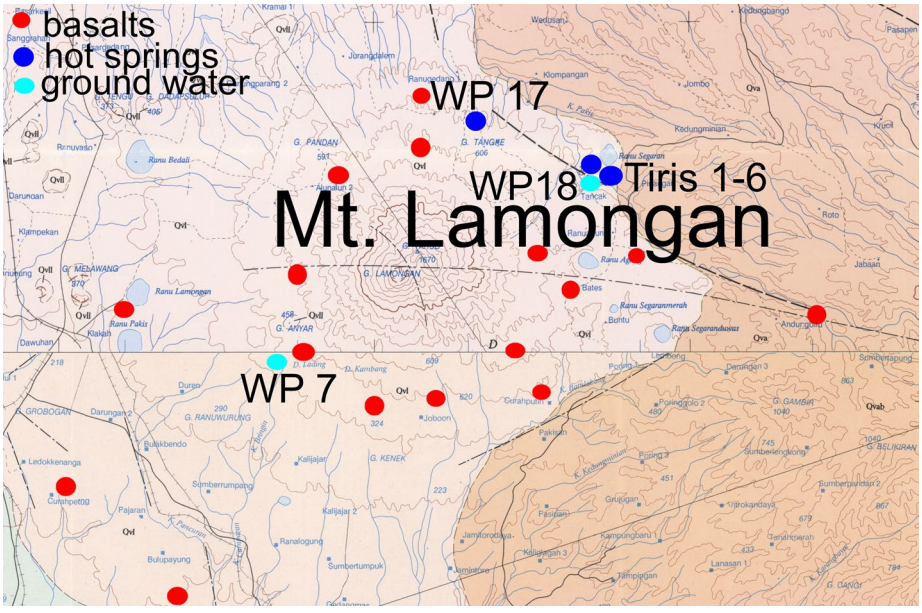


**Fig. 2** Magnified map of the investigation area around the Lamongan Volcano: *red circles* indicate the location of the rock samples, *light blue circle* the ground water samples and the *dark blue circle* the hot springs. The region is characterized by the occurrence of two volcanic complexes, the Lamongan and Argopuro

Java is located on the Sunda Arc that forms part of the Indonesian Archipelago between the landmasses of Eurasia and Australia at the NE margin of the Eurasian Plate. The Sunda Arc is a volcanic belt that has formed as result of the subduction of the Indo-Australian Plate beneath the Eurasian Plate, with a rate of ~6 cm $a^{-1}$ (Hamilton 1979; Puspito and Shimazaki 1995). It extends from the Andaman Islands north of Sumatra to the Island of Alor in the Banda Sea, covering a distance of more than 3000 km (Carn and Pyle 2001). Subduction in the Sunda Arc started in the early Eocene (Katili 1975; Hamilton 1979; Rangin et al. 1990). Java hosts 90 Holocene volcanoes, with the Merapi in West Java as one of most active volcanoes worldwide. An E–W trending chain of more than 30 modern volcanoes forms the central spine of Java. The rocks building up the volcanoes classify as tholeiitic, calc-alkaline, and high-K calc-alkaline and alkaline suites (Whitford et al. 1979). Basalt and basaltic-andesite constitute the dominating rock types, mainly composed of anorthitic plagioclase, pyroxene, and minor olivine.

Smyth et al. (2008) divide Java's major geological provinces as follows:

(1) The early Cenozoic mountain arc: today uplifted and partially eroded. It is one of the few exposures of arc-related crystalline basement built up by Cretaceous ophiolites. Arc rocks are thick (>2500 m) and are spread over a distance of 50 km.
(2) The Kendeng basin: this poorly exposed region is characterized by a strong negative Bouguer anomaly, which extends all the way to Bali. This anomaly becomes less negative around the modern volcanic arc. It is E–W oriented for at least 400 km parallel to the southern mountains. It is filled by volcanoclastic turbidites and pelagic mudstones.

(3) The Sunda shelf: the area was explored for hydrocarbon exploration. Between 2000 and 6000 m of Eocene to Pliocene shallow marine clastic and extensive carbonate sedimentary rocks were deposited within fault-controlled basins.

### Mount Lamongan

Lamongan volcanic field (LVF) of East Java represents a volcanic region with numerous cindered cones and maars. The LVF is situated at the transition zone between the compression-dominated subduction zone to the south and the extension-dominated back-arc region Masalima to the north, forming the Java Sea. Two previous studies (Carn 2000; Carn and Pyle 2001) investigated the morphologic, petrologic and geochemical characteristics of the maars and cindered cones, but did not involve geothermal field studies. Maars and cindered cones formed when magmas came in contact with water, causing a phreatomagmatic eruption associated with pyroclastic fallouts and flow deposits (Heiken 1971; Fisher and Waters 1970; Moore et al. 1966). Some of the maars in the Lamongan area are NW–SE oriented, comparable with the strike of the Tiris fault (Carn 1999). The Lamongan volcano is located in a structurally complex area and was very active until approximately 14,000 years ago. The volcano is composed of three different vents: Tarub, Tjupu and Lamongan itself (Carn 1999). Tarub is the oldest cone and detached from the younger stratocone of Lamongan by a prominent NW–SE depression, which is most likely fault related. Recent studies have shown that Lamongan belongs to the reviving volcanoes in Indonesia, as seismic activities have recently increased (Chaussard and Amelung 2012).

Tiris is a small village located on the eastern flank of Mount Lamongan. Several warm springs occur in close proximity. They have temperatures ranging between 35 and 45 °C (Deon et al. 2012, 2013), which are ~10 °C warmer than the surrounding groundwater. Because of this temperature difference, we supposed that the area hides a geothermal potential hard to be exploited due to the difficult field conditions.

Rainwater may have been trapped in the pyroclastite layers and could have build horizons which previously interacted with the magma beneath the Lamongan and possibly represents one part of the fluids available in the area. One should consider the location of LVF approximately 20 km from the coast. In the area, several lineaments and faults are known (Carn 1999). Thus, it is beyond doubt that a considerable water infiltration may have occurred sometime in the past.

### Topography, morphology, and hydrogeology

The area of Mt. Lamongan is characterized by a steep terrain landscape and dense tropical vegetation. Geological mapping of the area is challenging due to difficult access and the occurrence of severely weathered rocks at the surface. For instance, the outcropping basaltic rocks experienced intense lateritization. Heavy rain from December to May and a dry period from May to October characterize the climate in East Java. Moreover, significant variation of the precipitation rate exists depending on the elevation area. The annual precipitation in Pasuruan approximately 40 km NW of the study area at 15 m above sea level (a.s.l.) is 1300 mm/year. In Klakah, situated S of Mt. Lamongan at 250 m a.s.l., it is about twice that much, i.e., 2400 mm/year (Sporrer 1995). The steep area is sparsely populated and access to outcrops and hot springs is difficult. The fluid sampling

locations refer to the following altitudes (a.s.l.): springs Tiris 1 to Tiris 6 = 510 m; spring WP7 = 382 m.

## Methods

### Field work and sampling

The fieldwork around the Lamongan area covered an area of about 16 $km^2$ and included the systematic structural measurement of the strike direction of fractures. In particular, fractures were measured in the area around Lamongan after the last volcanic activity in March 2012. Lineaments could not be recognized in the field, but are evident in aerial photographs.

Magmatic rocks were sampled around Mt. Lamongan volcano; water samples were collected from the main river (Tancak), springs, maars, and from the sea (outside the investigation area; Figs. 1, 2). The springs Tiris 1–6 are located along the Tancak river. Water samples were collected from seven warm springs both east (Tiris 1–6) and northeast of the volcano (WP17), the Tancak river (WP18), and from the lake Ranu Lading (WP7 lad). Seawater was sampled on the coast north of the town Probolinggo (WP5). Figure 2 compiles the sampling sites around the volcano. The water samples were collected according to the procedure of Giggenbach and Goguel (1989) and Marini (2000) recommended for the quantitative analysis of the major ions and isotopes of oxygen, hydrogen, and strontium. Water samples were filtered using a 0.45 µm membrane filter to prevent the interaction of the fluid with suspended particles and algal growth. For the analysis of anions and isotopes, water samples were untreated, while for cation analysis, the water samples were acidified with $HNO_3$. Water samples collected for major ions and Sr-isotope analyses were stored in small polyethene bottles, while for isotope analysis of H and O, the samples were stored in glass bottles.

The sampling was undertaken twice every year since November 2010. One campaign took place in the dry season (from May until October), while the other was performed in the rainy season (from November until May), to observe seasonal variation due to the varying rates of precipitation. The on-site measurements conducted in the different seasons covered pH, temperature (T), electrical conductivity, and carbonate content (Table 1). Also measured were the contents of total dissolved solids (TDS), salinity, and

**Table 1 Mean values of the field parameters of water samples**

| Sample | | T (°C) | pH | Conductivity (µS/m) | TDS (mg/L) | Salinity (g/L) | Altitude (m a.s.l.) |
|---|---|---|---|---|---|---|---|
| WP17 | Spring | 35.0 | 7.60 | 1849 | 91 | 0.09 | 382 |
| Tiris 1 | Spring | 38.0 | 7.02 | 1707 | 1100 | 1.10 | 510 |
| Tiris 2 | Spring | 44.5 | 7.19 | 2850 | 900 | 1.10 | 510 |
| Tiris 3 | Spring | 44.0 | 7.10 | 2890 | 1450 | 1.48 | 510 |
| Tiris 4 | Spring | 44.0 | 7.10 | 2760 | 1380 | 1.42 | 510 |
| Tiris 5 | Spring | 36.2 | 7.15 | 2590 | 1250 | 1.30 | 510 |
| Tiris 6 | Spring | 34.3 | 7.20 | 2250 | 1130 | 1.14 | 510 |
| WP 7 | Lake | 29.0 | 7.00 | 1606 | 803 | 0.7 | 320 |
| WP 18 | River | 27.0 | 7.00 | n.d | n.d | n.d. | 510 |
| WP5 | Sea | 29.0 | 7.00 | n.d. | n.d. | n.d. | 0 |

Conductivity reported is a mean value based on the field campaigns

*TDS* total dissolved solid in the liquid

bicarbonate (measured by titration with a stripe test). The chemical water analyses were conducted at the Geochemistry Laboratory, Department of Applied Geosciences, and Technical University Berlin, Germany. Anion concentrations ($Cl^-$, $SO_4^{2-}$) were measured with an Inductively Coupled Plasma Atomic-Emission Spectrometer (ICP-AES; Thermo iCap 6300), while the cations ($Ca^{2+}$, $Mg^{2+}$, $K^+$, $Na^+$, $Fe^{2+}$, $Si^{4+}$, $Li^+$, $Rb^+$, $B^{3+}$) were determined by Atomic Absorption Spectrophotometry (AAS). Isotope measurements were conducted on a selection of water samples (cf. "X-ray fluorescence analysis (XRF)", "Stable-isotope (D–O) analysis"). The uncertainty of the measurements is ~0.05 ppm.

#### Electron microprobe analysis (EMPA)

Single-spot mineral analyses were performed using a CAMECA SX100 electron microprobe operating in the wavelength-dispersive mode at the Electron Microprobe Laboratory, Department of Inorganic and Isotope Geochemistry at the Helmholtz Centre Potsdam—German Research Centre for Geosciences (GFZ) in Potsdam, Germany. The analytical conditions include an accelerating voltage of 15 kV, a beam current of 10 nA, and a focused beam. Well-characterized grains of plagioclase, olivine and pyroxene were used as standards. Secondary-electron (SE) images were collected with a JEOL JXA 8230 electron microprobe (15 kV accelerating voltage) in the same laboratory.

#### X-Ray diffraction analysis (XRD)

To determine the modal mineralogy of the rocks by XRD, the rock samples were crushed and sieved to obtain the 63-µm fraction. XRD patterns were recorded in transmission using a fully automated STOE STADI P diffractometer (Cu-$K_\alpha$ radiation), equipped with a primary monochromator and a 7°-wide position sensitive detector, at the Department of Chemistry and Physics of Earth Materials at GFZ. The diffractograms were refined with the EXPGUI-GSAS software (Larson and Von Dreele 2000; Toby 2001; Belsky et al. 2002), using reference structures from the ICDS database (Bergerhoff and Brown 1987). Additional X-ray measurements (step-scan mode) were performed with an automatic Siemens D500 diffractometer (half automatic beam—40α, Graphite secondary monochromator—with Cu $K_\alpha$ 40 kV, 35 mA) at the Section of Material Research and Physics, University of Salzburg, Austria.

#### X-ray fluorescence analysis (XRF)

XRF analyses were conducted at the Department of Inorganic and Isotope Geochemistry at Helmholtz Centre Potsdam—German Research Centre for Geosciences, using a PANanalytical AXIOS instrument featuring a 4 kW Rh tube. Additional XRF data were acquired at the Section of Material Science and Physics, University of Salzburg, on a Bruker S4 Pioneer instrument, equipped with a 4 kW Rh tube. Major elements were determined at reduced tube energies. Counting times were chosen such that the relative 2σ uncertainties were less than 1 % for Si and Al, and less than 5 % for elements occurring at the 1–10 wt% concentration level. For the determination of trace elements, tube conditions and counting times were optimized automatically up to 4 kW and 400 s per element, to obtain a detection limit of ~3 ppm (3σ). Typical errors (2σ) from

the counting statistics were 1–2 ppm at low concentrations (<10 ppm), ~5 ppm at the 100 ppm concentration level, and better than 50 ppm at the 1000 ppm level.

#### Stable-isotope (D–O) analysis

δ D and δ $^{18}$O measurements were performed at Alfred Wegner Institute, Helmholtz Centre for Polar and Marine Research, Potsdam, Germany. The water samples (3 mL) were analyzed using a Finnigan MAT Delta-S mass spectrometer equipped with two equilibration units for the simultaneous determination of hydrogen and oxygen-isotopic composition. In one sequence, 48 water samples (including standards) were measured in two equilibration units with 24 sample positions each. The first position of each unit was equipped with the measuring standard water. Three standards were used for quality control. Measuring and control standards were selected according to the expected isotopic composition of the samples. The isotope data were corrected linearly compared to the standards if necessary. The 1σ standard deviation ranges from 0.03 to 0.08 (O) and from 0.2 up to 0.8 (D).

#### Sr-isotope analysis

Sr-isotope measurements of rocks (basalts and carbonates) and waters were performed at Geosciences Centre, University of Göttingen, Germany. For Sr-isotope analysis of volcanic rocks, about 100 mg of powdered samples was digested in a mixture of 40 % HF and 65 % $HNO_3$ at 100 °C. After complete dissolution and evaporation, the sample residue was dissolved in 6 N HCl at 100 °C and again evaporated. The sample residue was then re-dissolved in 2.5 N HCl for further treatment using ion-exchange chromatography. For the analysis of thermal waters, about 2 mL of water was evaporated and re-dissolved in 2.5 N HCl. A sample of $CaCO_3$ was directly dissolved in 2.5 N HCl. Separation of Sr from other cations was done on quartz-glass columns using Biorad AG 50 × 8 (200–400 mesh) resin and 2.5 N HCl. Purified Sr-fractions were loaded onto outgassed Re filaments using 0.25 N $H_3PO_4$ and measured on a Finnigan MAT262 thermal ionization mass spectrometer (TIMS). $^{87}Sr/^{86}Sr$ ratios were corrected for instrumental fractionation using the natural $^{88}Sr/^{86}Sr$ ratio of 8.375209. Routine standard measurements yielded an average $^{87}Sr/^{86}Sr$ ratio of 0.71040 ± 0.00002 (2σ: $n = 15$) for the NBS987 standard. Only distilled reagents were used for chemical sample preparation. Blanks were less than 0.5 ng for Sr. The reproducibility of the individual $^{87}Sr/^{86}Sr$ ratio was equal to or less than 0.00003 (2σ).

## Results

#### Water chemistry

The concentrations of major cations and anions of ground, river, and thermal waters are listed in Table 2. Surface water temperatures range between 27 and 29 °C. The sampled thermal springs have temperatures ranging from 35 to 45 °C; pH values are between 7.0 and 7.6. EC values vary from 1710 µS/cm (spring Tiris 1) to 2890 µS/cm (spring Tiris 3). Major ions in sampled water are Mg, Na, Cl, and $HCO_3$. Highest values of up to 2100 mg/L $HCO_3$ occur in spring water, while lake and river water show lower concentrations of maximum 427 mg/L. The samples Tiris 1–6 show a higher Mg content

**Table 2 Chemical composition (mg/L) and stable-isotope and $^{87}Sr/^{86}Sr$-composition of ground and thermal waters sampled during the field campaigns**

| Sample | | Ca | Mg | K | Na | Fe | Li | Rb | Si | B | $Cl^-$ | $HCO_3^-$ | $SO_4^{2-}$ | Ionic balance | $^{18}O$ | $^{2}H$ | $^{87}Sr/^{86}Sr$ |
|---|---|---|---|---|---|---|---|---|---|---|---|---|---|---|---|---|---|
| WP17 Oct 2012 | Spring NE | 33.5 | 37.4 | 44.1 | 249 | 0.0 | 0.0 | 0.2 | 26.1 | 4.9 | 330 | 632 | 0.0 | −19[a] | −5.85 | −31.4 | n.d. |
| Tiris 1 June 2012 | Spring E | 63.9 | 159 | 49.0 | 273 | n.d. | 0.29 | 0.17 | 68 | 14 | 355 | 1280 | 23.8 | −3 | −5.8 | −36.9 | 0.70464 (±3) |
| Tiris 2 June 2012 | Spring E | 93.5 | 227 | 76.5 | 406 | n.d. | 0.39 | 0.28 | 83 | 21 | 521 | 2100 | 23.1 | 6 | −5.1 | −35.5 | 0.70464 (±2) |
| Tiris 3 June 2012 | Spring E | 86.1 | 201 | 69.1 | 370 | n.d. | 0.35 | 0.26 | 77.6 | 20 | 465 | 1650 | 23.2 | −2 | −5.06 | −36.9 | n.d. |
| Tiris December 2011 | Spring E | 80.3 | 168 | 67.1 | 353 | 1.30 | 0.47 | 0.28 | 65.0 | 13.2 | 441 | 1340 | n.d. | 1 | n.d. | n.d. | n.d. |
| Tiris 5 June 2012 | Spring E | 61.9 | 222 | 45.7 | 268 | n.d. | 0.22 | 0.16 | 70.4 | 14 | 130 | 1680 | 4.63 | 4 | −5.28 | −33.9 | n.d. |
| Tiris 6 December 2012 | Spring E | 54.3 | 192 | 43.9 | 254 | n.d. | 0.3 | 0.2 | 57.8 | 10.3 | 348 | 1400 | n.d. | −3 | −5.49 | −36.5 | n.d. |
| WP7 Lad June 2012 | Lake | 39.7 | 34.0 | 8.0 | 33.3 | n.d. | 0.0 | 0.0 | 20.4 | 2.0 | 8.1 | 427 | 15.0 | −8 | n.d. | n.d. | n.d. |
| WP18 June 2012 | River | 29.1 | 17.1 | 4.7 | 17.4 | n.d. | 0.0 | 0.0 | 32.5 | 0.0 | 11.9 | 323 | 11.0 | −12 | n.d. | n.d. | n.d. |
| WP 5 June 2012 | Diluted and contaminated seawater | 257 | 963 | 282 | 773 | n.d. | 0.0 | 0.2 | 4.2 | 2.0 | 12,800 | 610 | 2450 | 1 | n.d. | n.d. | n.d. |

[a] Sampling of WP17 was additionally conducted by the Indonesian project partners. Their sampling yielded similarly poor ionic balances, with the value scattering between −19 and −22. The poor quality of the ionic balance is due to anthropogenic activities of a nearby village (approximately 1 km)

compared to the others: Tiris 2 contains 227 mg/L. The other samples are characterized by a lower Mg content, with the exception of WP5, diluted sea water, which contains 963 ppm. Highest cation-concentrations are Na with values of 406 mg/L in spring water and 774 mg/L in seawater. Spring and surface water are most distinct with respect to the Cl concentration (Table 2). $\delta^2H$ and $\delta^{18}O$ values plot along the meteoric water line (Fig. 3) and range between −5.06 and −5.85 for $\delta^{18}O$ and −31.4 and −36.9 for $\delta^2H$. No significant trend can be recognized, indicating that the values refer to pure rain water.

The Giggenbach ternary diagram (Fig. 4a, b) shows that sampled waters plot in the area of peripheral waters, due to low $SO_4$ and high $HCO_3$ concentrations. The warm spring Tiris 2 contains ~20 % more Cl than the WP7 spring along the river (WP 18), which shows higher $HCO_3^-$ concentrations. The seawater sample (WP 5) plots in the area of mature waters (Fig. 4a).

As indicated in the Giggenbach and Piper diagrams (Fig. 5), the correlation plot (Fig. 6a) Cl over B shows a clustering of spring samples Tiris 1–6 compared to hot spring sample WP 17. This separation is also obvious in the Cl/B-ratio, which is high (82) for WP 17 and lower (20–34) for Tiris 1–6. The clustering is not that obvious in the Cl/Na plot. However, a clear positive correlation exists between the concentrations of Cl and Na, as being the major conservative ions. Highest concentrations occur in seawater sample WP 5. However, with 12.8 g/L, the content is still below mean seawater concentration of 19 g/L. Similar clustering has been observed in the Cl/Si plot (Fig. 7a), with Tiris 1–6 springs show higher concentrations than WP17. While Cl concentrations are less variable, comparably higher variations in Si concentrations are due to closer location to the heat source, where fluids show increased chemical reactions with host rock.

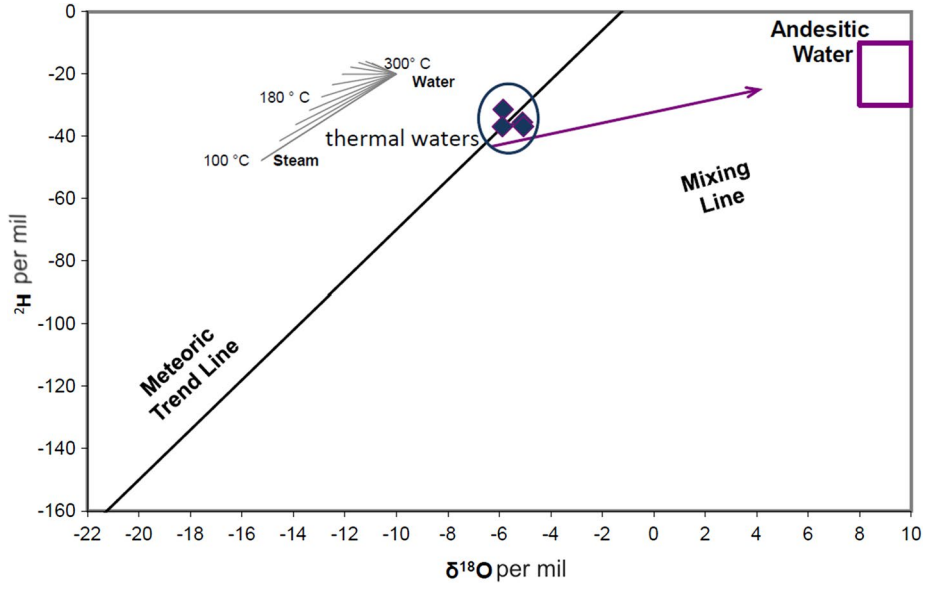


**Fig. 3** *Plot* showing the stable-isotope measured $^{18}O$ vs. $^2H$ measured on the warm springs samples and plotted with the meteoric water reference. A significant trend cannot be recognized as the samples lie all very close to the meteoric line. No relevant information can be obtained about water–rock interaction

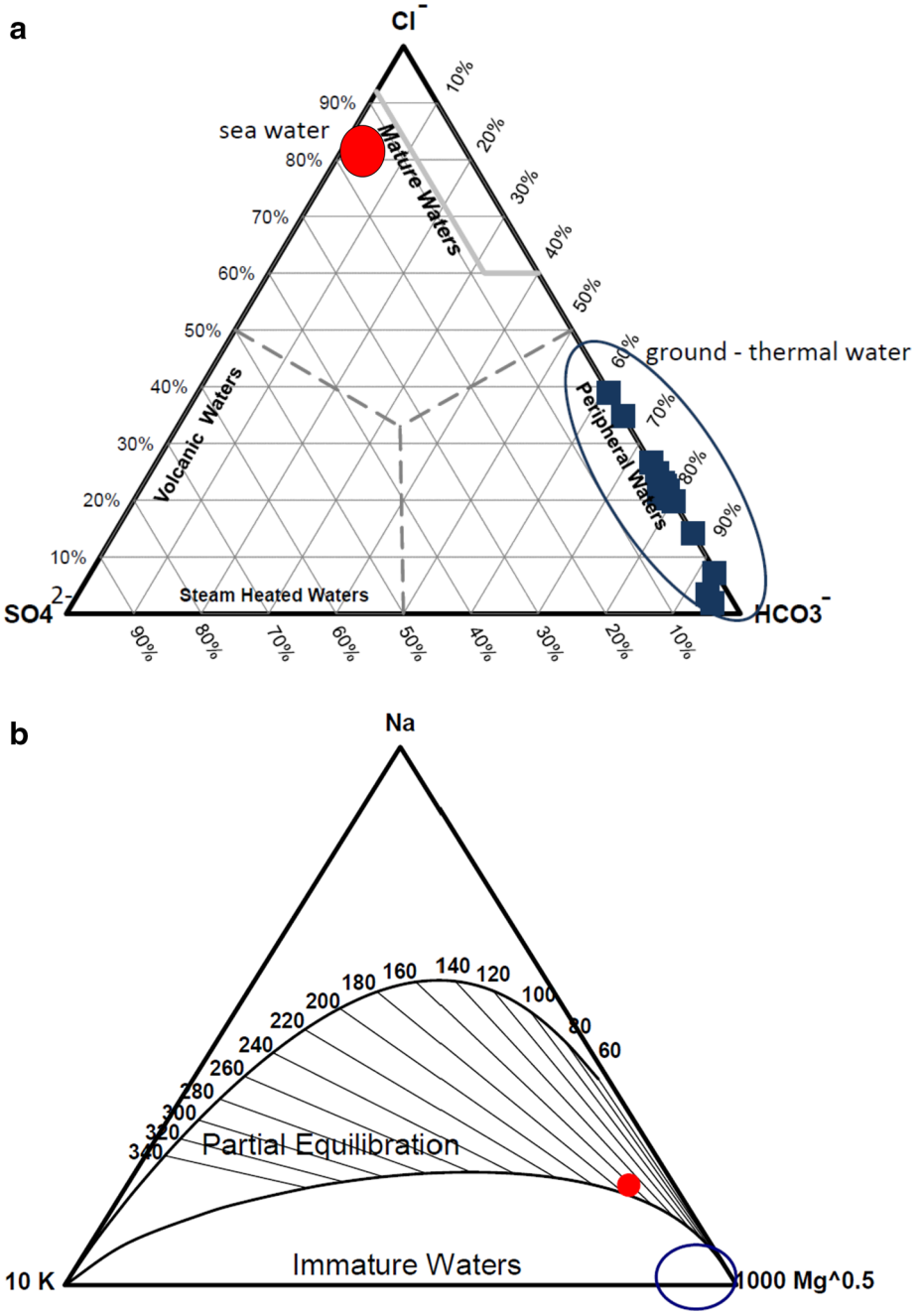


**Fig. 4** **a** Ternary plot of the major anions $Cl^{-}$, $SO_4^{2-}$, $HCO_3^{-}$. The fluid samples in Tiris show an excess in bicarbonate, relatively high to moderate Cl and no sulfate. The slight differences in the concentrations are due to seasonal changes, e.g., rainy and dry season. According to the diagram, the waters can be classified as immature. **b** Ternary plot of the major cations (Na, K, Mg). The cation values were clustered as they show very similar values. Both *plots* indicate that the springs may belong to an outflow-recharge area of the system. The absence of sulfate may be connected to the spring location in the outflow area of the system

### Geothermometric calculations

Mg, Ca, Na, and K concentrations in spring water show that the rising waters are not in equilibrium. Therefore, cation geothermometers are not applicable. However, the use of

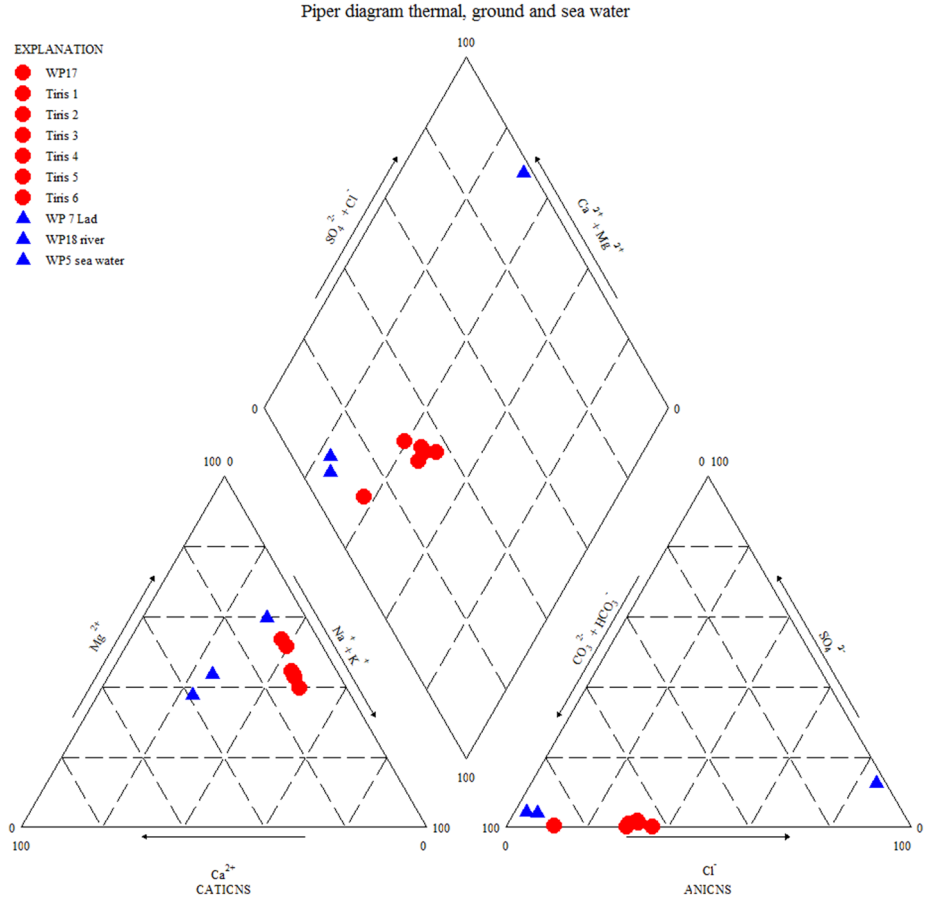


**Fig. 5** Piper diagram of the thermal, ground and sea water developed with the major cations, anions and TDS of the fluid samples. A comparison with other springs is the area is not possible due to inaccessible data for publication

quartz geothermometers (Fournier 1989) requires assumptions about the quartz mineral species whose solubility is controlled dominantly by fluid/rock temperature. Plotting $SiO_2$ over $\log(K^2/Mg)$ helps to identify the dominant species. In our case, the main controlling species is chalcedony (Fig. 7b). Therefore, reservoir temperatures have been calculated based on hot spring samples using the chalcedony conductive, quartz conductive and quartz adiabatic geothermometers (Table 3). Calculated temperature using chalcedony geothermometer ranges between 107 and 140 °C. These temperatures are considered as minimum values because the deep hot fluids can have been partially diluted by colder shallow, Si-poor freshwaters during their ascent to surface, as suggested by Figs. 6a, b, 7a, b.

### Mineralogy and petrology of the volcanic rocks

In the Total Alkali Silica (TAS) diagram adapted from Le Bas et al. 1986, the Lamongan rocks plot in the field of basalt. The basalts, derived from different episodes of effusive activity of Lamongan, are mainly composed of plagioclase ($An_{65}$–$An_{90}$) accompanied by minor olivine and pyroxene (Figs. 8a, b, 9a–c; Tables 4, 5). In fresh samples, plagioclase grains are several mm in size, twinned, and virtually unaltered (Fig. 9a–c).

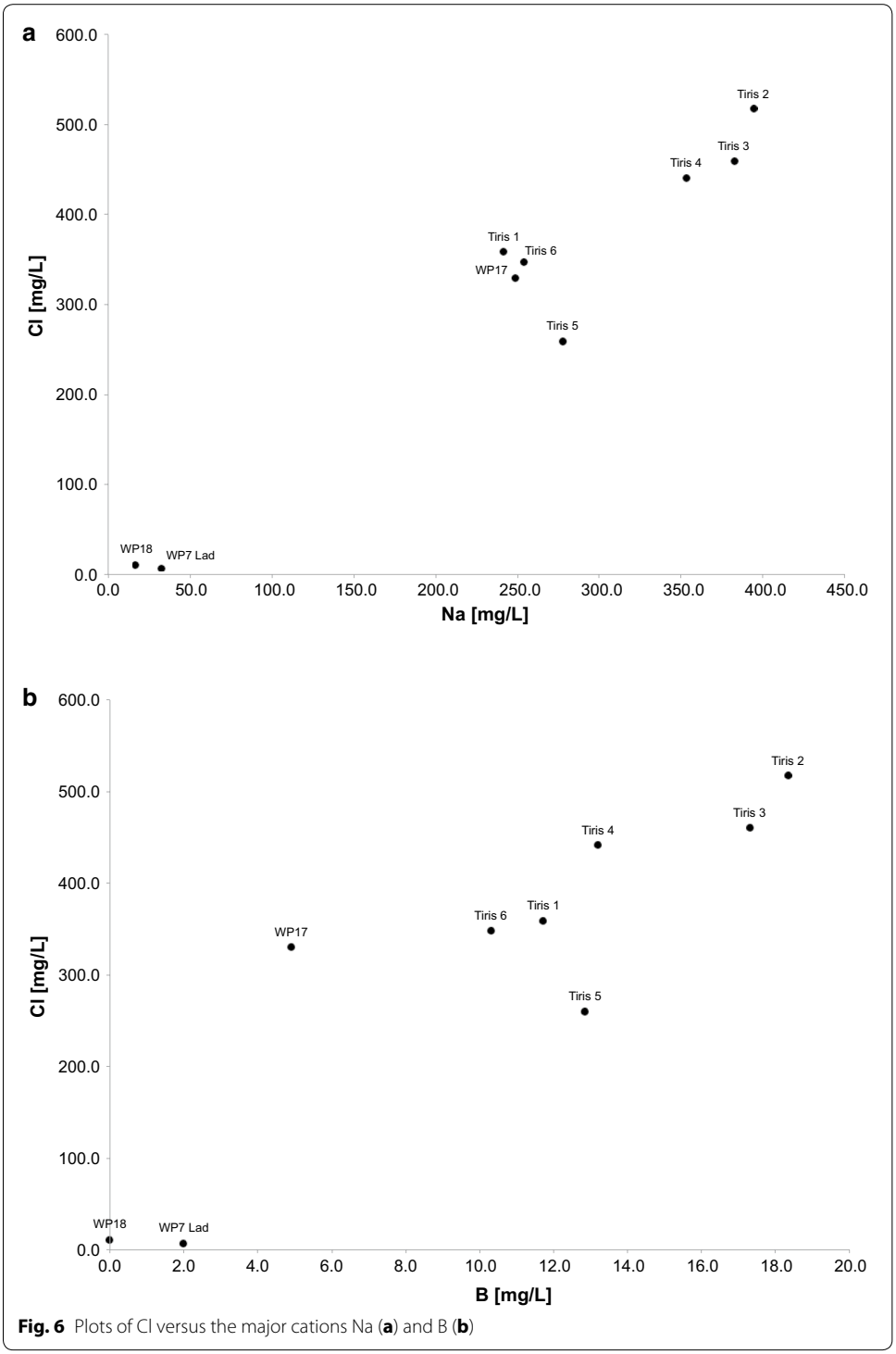


**Fig. 6** Plots of Cl versus the major cations Na (**a**) and B (**b**)

Major-element composition of bulk rock is shown in Table 4. The basalts are characterized by low concentrations of Si (46–50 wt% $SiO_2$) and alkali elements (1.6–2.9 wt% $Na_2O$, 0.63–2.3 wt% $K_2O$) and are high in Ca (7–11 wt% CaO) (Fig. 10). The narrow range in Si indicates that the subsequently extruded magmas in this area experienced a relatively low degree of differentiation. $^{87}Sr/^{86}Sr$ initials range from 0.70430 (WP11) to 0.70463 (FD8).

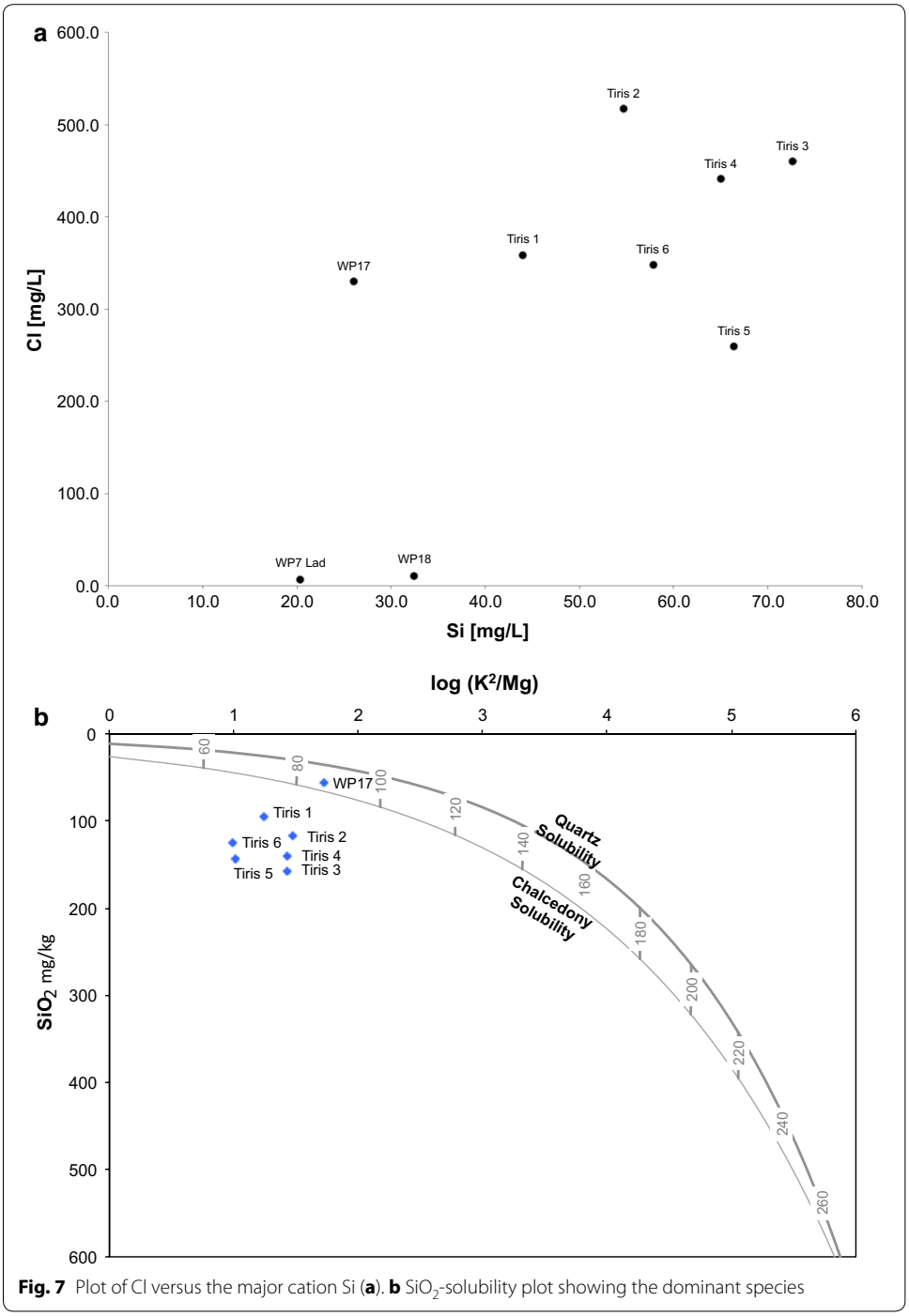


**Fig. 7** Plot of Cl versus the major cation Si (**a**). **b** $SiO_2$-solubility plot showing the dominant species

## Discussion

### Rock petrology

The $^{87}Sr/^{86}Sr$ ratio of the weakly fractionated basalts varies between 0.70430 and 0.70463 and recalls the values of basalts close to the Sunda arc minimum (i.e., Whitford et al. 1979). It is generally accepted that the $^{87}Sr/^{86}Sr$ ratio of the volcanic rocks decreases from West Java to Bali. A model proposed by Sisson and Bronto (1998) presumes a mantle

**Table 3 Silica-geothermometers applied to the water samples**

| Sample | Chalcedony cond. | Quartz cond. | Quartz adiabatic |
|---|---|---|---|
| WP17 | 77 | 107 | 107 |
| Tiris 1 | **107** | **134** | **130** |
| Tiris 2 | **120** | 146 | 140 |
| Tiris 3 | **140** | 164 | 155 |
| Tiris 4 | **132** | 157 | 149 |
| Tiris 5 | **134** | 158 | 150 |
| Tiris 6 | **124** | 150 | 143 |
| WP7 Lad | **65** | 96 | 97 |
| WP18 | **89** | 118 | 116 |
| WP 5 | 3 | **34** | **44** |

The numbers in bold are the most likely reservoir temperatures (in °C). Calculated following Fournier (1989)

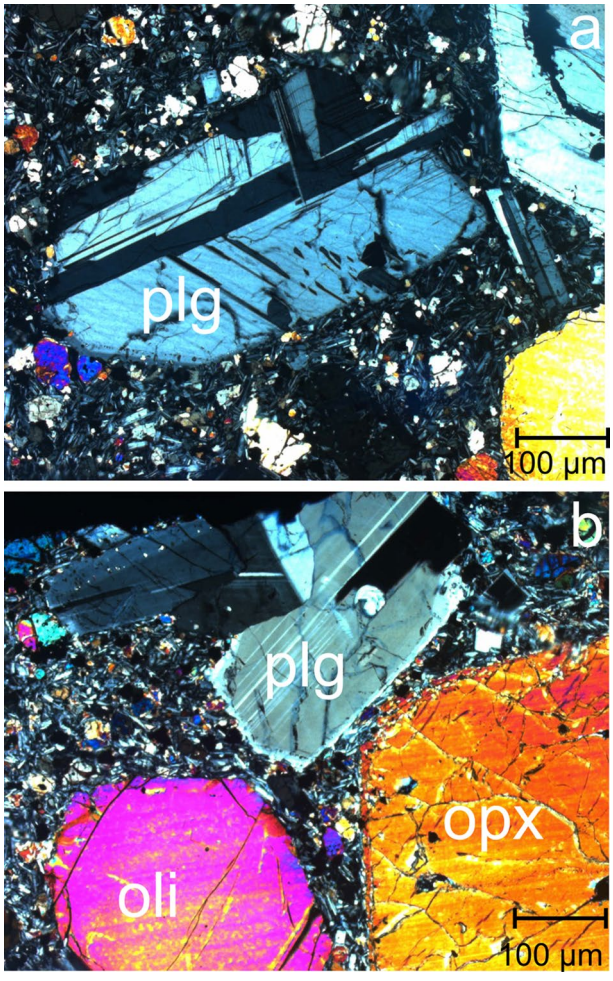


**Fig. 8** Microphotographs from optical microscopy. **a** Unaltered plagioclase crystals showing twinning. **b** Fractured olivine, orthopyroxene and plagioclase (with twinning) grains in lava WP11

upwelling that has initiated a pressure release beneath the Lamongan Volcano. Mantle upwelling combined with the extensional tectonic characterizing East Java gave rise to a locally thinned crust. The presence of one or more shallow magma chambers between 1

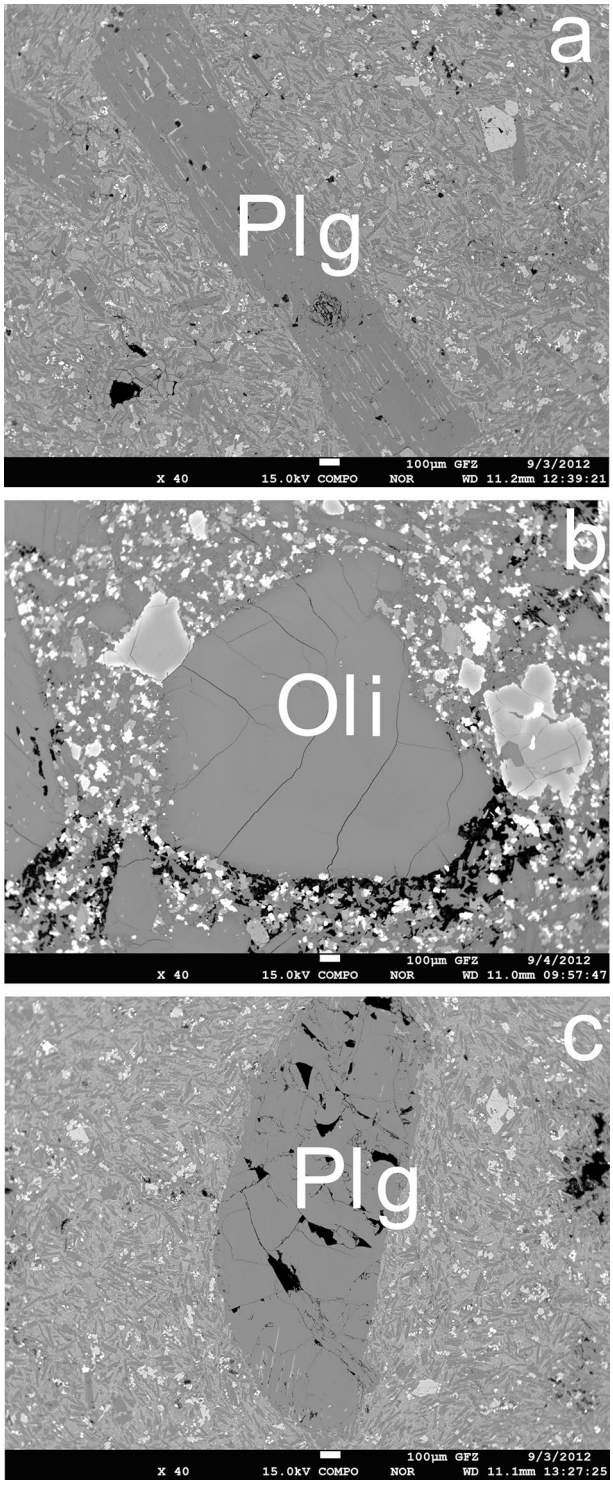


**Fig. 9** Secondary-electron images collected with the electron microprobe. **a** Elongated euhedral plagioclase in a microcrystalline matrix. **b** Fractured olivine surrounded by magnetite (bright). **c** Fractured plagioclase grain with elongated habitus in a microcrystalline matrix

**Table 4 Bulk rock composition (wt%) of basalts and carbonates and their initial Sr-isotopic signature**

| Sample | $SiO_2$ | $TiO_2$ | $Al_2O_3$ | $Fe_2O_3$ | MnO | Mg | CaO | $Na_2O$ | $K_2O$ | $P_{25}$ | Total | $^{87}Sr/^{86}Sr$ |
|---|---|---|---|---|---|---|---|---|---|---|---|---|
| FD1 | 46.1 | 1.37 | 19.1 | 12.9 | 0.20 | 4.58 | 10.9 | 2.73 | 0.85 | 0.08 | 99.7 | – |
| FD8 | 50.3 | 1.63 | 15.6 | 13.4 | 0.20 | 3.27 | 8.11 | 2.53 | 1.61 | 0.39 | 99.6 | 0.70463 (±2) |
| WP2 | 47.0 | 1.09 | 19.4 | 12.1 | 0.19 | 4.99 | 10.8 | 2.48 | 0.63 | 0.11 | 99.7 | 0.70447 (±3) |
| WP9 | 49.4 | 1.06 | 17.9 | 10.9 | 0.16 | 2.68 | 7.86 | 2.86 | 2.26 | 0.38 | 99.7 | 0.70447 (±2) |
| WP8 | 50.0 | 2.00 | 14.4 | 15.5 | 0.25 | 3.87 | 7.68 | 2.54 | 1.90 | 0.53 | 99.6 | 0.70445 (±2) |
| WP11 | 47.2 | 1.20 | 19.0 | 12.7 | 0.20 | 4.67 | 10.4 | 2.65 | 0.64 | 0.17 | 99.8 | 0.70430 (±1) |
| WP12 | 44.9 | 0.92 | 15.3 | 12.7 | 0.19 | 10.8 | 11.8 | 1.56 | 0.29 | 0.09 | 99.8 | 0.70449 (±1) |
| WP14 | 50.7 | 0.99 | 20.0 | 9.3 | 0.15 | 2.75 | 8.21 | 2.85 | 2.12 | 0.41 | 99.7 | 0.70428 (±2) |
| WP17 | 46.0 | 1.32 | 19.2 | 12.8 | 0.20 | 4.92 | 11.2 | 2.67 | 0.84 | 0.09 | 99.7 | 0.70464 (±3) |
| WP13 | 47.2 | 2.03 | 16.7 | 14.4 | 0.26 | 2.77 | 9.83 | 2.72 | 1.19 | 0.46 | 100.0 | – |
| WP19 | 50.5 | 0.94 | 19.9 | 11.2 | 0.18 | 3.20 | 8.71 | 3.26 | 1.09 | 0.24 | 100.0 | – |
| WP20 | 51.6 | 0.94 | 20.6 | 10.1 | 0.18 | 2.41 | 9.44 | 3.62 | 0.97 | 0.15 | 100.0 | – |
| WP22 | 48.8 | 1.04 | 21.0 | 10.7 | 0.18 | 3.51 | 10.8 | 3.17 | 0.66 | 0.09 | 99.9 | – |
| WP4a[a] | 0.4 | 0.00 | 0.13 | 0.08 | 0.01 | 0.21 | 54.7 | 0.05 | 0.00 | 0.00 | 99.8 | – |
| WP4b[a] | 4.4 | 0.08 | 1.99 | 0.87 | 0.01 | 0.47 | 50.8 | 0.06 | 0.04 | 0.00 | 100.0 | – |

[a] Carbonate rocks sampled outside the research area

**Table 5 Modal composition (wt%) of basalts**

| Sample | Rock type | Plagioclase | Olivine | Clinopyroxene | Orthopyroxene | Calcite | Chlorite |
|---|---|---|---|---|---|---|---|
| FD1 | Basalt | Labradorite 94 | 6 | – | – | | |
| FD8 | Basalt | Labradorite 86 | 13 | Diopside 1 | | | |
| WP2 | Basalt | Labradorite 72 | 28 | | | | |
| WP9 | Basalt | Labradorite 71 | 29 | | | | |
| WP8 | Basalt | Labradorite 63 | 37 | | | | |
| WP11 | Basalt | Labradorite 79 | 21 | | | | |
| WP12 | Basalt | Labradorite 42 | 57 | | | 4 | |
| WP14 | Basalt | Labradorite 83 | 17 | | | | |
| WP 17 | Basalt | Labradorite 71 | 29 | | | | |
| WP13 | Basalt | Andesine 50 | | Diopside 18 | Augite[a] 28 | | |
| WP19 | Basalt | Andesine 68 | | Diopside 30 | | | 1 |
| WP20 | Basalt | Labradorite 68 | | Diopside 9 | Ferrosilite 23 | | |
| WP22 | Basalt | Labradorite 65 | | Diopside 14 | Ferrosilite 21 | | |

[a] Adopted from Carn and Pyle (2001)

and 3.5 km depth below Lamongan and Argopuro is geophysically constrained (Chaussard and Amelung 2012). A preliminary geological model assumes two volcanic complexes with a single magma chamber alimenting both edifices (Fig. 11). Whether one or two magma chambers occur underneath can be only confirmed by geophysical surveys along with deep drillings.

### Water composition

The thermal water sampled in the area can be classified, according to the Giggenbach diagram, as bicarbonate water. It is the first sampling in the area of Mt. Lamongan. However, springs from the nearby Argopuro volcanic complex show a higher sulfate

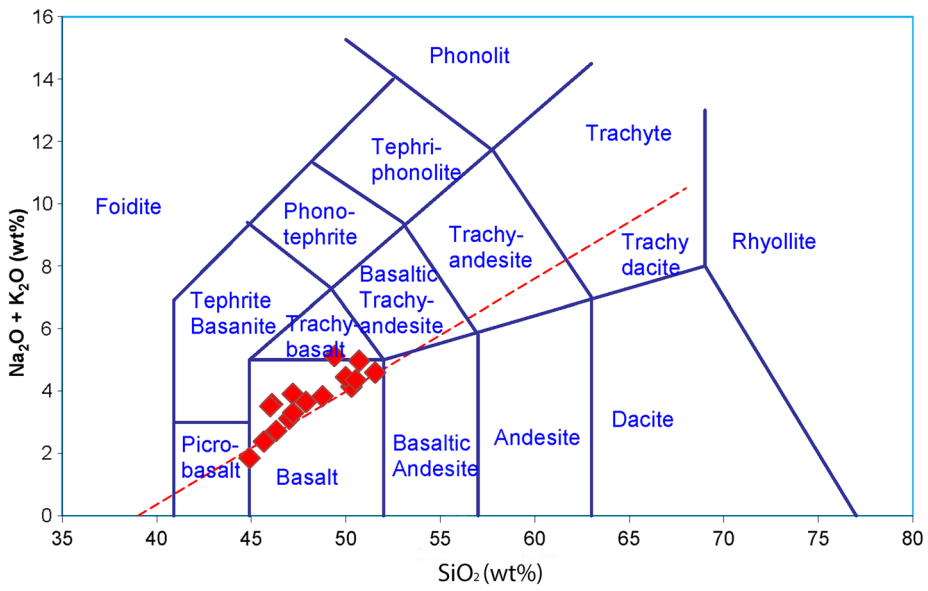


**Fig. 10** Total alkali vs. silica diagram of Le Bas et al. (1986). This diagram classifies our rock samples as basalts. The *red squares* refer to the samples of this study. The Lamongan basalts plot along the line, which divide alkaline and subalkaline domain. Note the small $SiO_2$ range of our samples, indicating low fractionation of the primitive magma

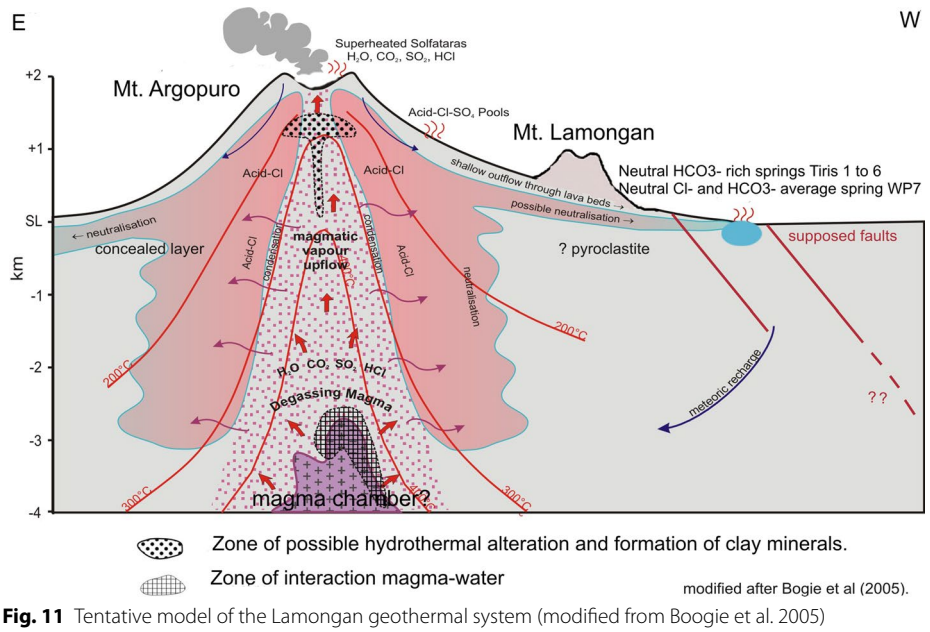


**Fig. 11** Tentative model of the Lamongan geothermal system (modified from Boogie et al. 2005)

content, higher temperatures and a lower pH (Pertamina Geothermal Energy 2015, pers. Comm.). This would indicate an active magma chamber and a heat source located beneath the Argopuro volcano and defines the Lamongan area as an outflow region from the Argopuro volcanic complex.

Isotope ratios show a basically meteoric origin of the sampled groundwater. High element concentrations and increased salinity are caused by strong alteration processes, along with high dissolution rates in the center of the geothermal field at Argopuro. Groundwater is transported and cooled down towards the discharge area and arises in hot springs, which show lower temperatures and higher $HCO_3$ concentrations. Relatively high Li and B concentrations are typical for basaltic-andesite rock formations (Nicholson 1993). Potassium shows concentrations typical for geothermal-alteration patterns, characterized by the formation of illite, smectite, or kaolinite (Brehme 2015). Low $SO_4$ values are due to the location of springs in the outflow zone. Sulfate minerals generally precipitate in low-pH springs occurring in the center of the geothermal field (Fig. 11). Generally, the WP 17 spring has slightly different Na/Cl ratios than Tiris 1–6 springs. Tiris 1–6 springs are located closer to the geothermal center, which let them cluster at higher concentrations of, i.e., Cl, Na, and B. It is interesting to note that the Mg content is elevated in the water from the springs in the proximity of the river running through basalts (Tiris 1–6). Their higher temperature facilitates the solution of Mg from these rocks.

The chalcedony geothermometer suggests a reservoir temperature of ~130 °C, which is reliable considering that the springs are located in an outflow area of a magmatically influenced system. Comparable systems, as the Lahendong geothermal field, which is controlled by young volcanism, show slightly higher reservoir temperatures in the center of the field (Brehme et al. 2014). However, the Lahendong field also shows temperatures of 140 °C in the outflow area (Brehme et al. 2014, 2015).

Kim et al. (2003) describe a geothermal setting similar to Tiris for the Jeju volcanic island in South Korea. The occurring lithologies share the properties of the rocks of the Tiris geothermal area: high permeable pyroclastites underlying less permeable basaltic lava. In the LVF, the pyroclastic units must have been derived from previous eruptions of Mt. Argopuro and the overlain fractured basalts are the products of the subrecent effusive activity of Mount Lamongan (nineteenth century). Faults and fractured rock play a major role in development of geochemical characteristics of the geothermal field (Brehme et al. 2015 submitted). Presumably, groundwater is migrating through the permeable pyroclastites, following pathways to the surface through predominant faults or fracture patterns. On its way to the surface, the water becomes slightly heated and equilibrated with the mafic rocks, as implied by the virtual identity of their $^{87}Sr/^{86}Sr$-isotopic composition. Interaction with a mantle-related source is further implied by the excess of $HCO_3^-$, since carbonate rocks are unknown in the study area and the only origin of $HCO_3^-$ could be explained by the degassing of mantle-derived magmas. This preliminary field study should be succeeded by subsurface exploration to improve the knowledge of the LVF geothermal system.

## Conclusions

The occurrence of highly permeable pyroclastites overlain by basalts supports the existence of a concealed layer, as described by Hochstein (1988), which could be responsible for capturing $H_2S$, accounting for the $HCO_3^-$ excess of the springs located in the outflow zone of the system. According to Chaussard and Amelung (2012), the Lamongan field belongs to the volcanoes with the world's highest uplift areas evidenced by InSAR data,

indicating magmatic activity in the subsurface. Lamongan might host potential hydrothermal resources, however, these are not expressed by surface manifestations, such as hot springs with $T > 50$ °C, steam grounds, or fumaroles as in other regions in Indonesia. The frequent occurrence of maars and cinder cones is related to the interaction of magma and hot water; however, the maar-water temperature is the same as the groundwater temperature in the area (29 °C). In addition to passive seismic recording and more comprehensive fluid sampling, shallow drillings are mandatory to evaluate the geothermal potential in this area. Lamongan likely constitutes the outflow area of a larger system, with the nearby Argopuro being the upflow area of this system. In this area, springs with substantially higher temperatures and lower pH values occur, fingerprinting the existence of an active magma chamber at depth. Due to concession and legal issues according to Indonesian law, these data are not open for publishing and thus, could not be used here. It becomes, therefore, challenging to link and proof the conclusions of this survey campaign. Our exploration study demonstrates that greenfield exploration based on hydrochemistry may fail to correctly evaluate the deep geothermal potential in tropical areas rich in meteoric water, and has to be succeeded by other site-specific exploration work.

**Authors' contributions**

FD carried out the field work, measurements and the interpretation. FD is the principal investigator. H-J F contributed to the interpretation of the rock geochemistry and gave relevant contribution in the manuscript writing. MB contributed to the water geochemistry interpretation and geothermometer application. BW carried out the strontium isotopes measurements and wrote the methods part related to this measurement. TS performed the cation and anion analyses on the water samples and supported the fluid chemistry interpretation. IM participated to the fieldwork and contributed to the geological interpretation. MSJ participated to the fieldwork. DP organized and supported the fieldwork. She is the leader of the oil and mineral resources agency for the province of Eastern Java. All authors read and approved the final manuscript.

**Author details**

[1] Delft University of Technology, Department of Geoscience and Engineering, Delft, The Netherlands. [2] Helmholtz Centre Potsdam GFZ, German Research Centre for Geosciences, Potsdam, Germany. [3] University of Göttingen, Göttingen, Germany. [4] Technical University of Berlin, Berlin, Germany. [5] Technical University of Munich, Munich, Germany. [6] SGS, Voorburg, The Netherlands. [7] DINAS ESDM, Surabaya, Indonesia.

**Acknowledgements**

The German Federal Ministry for Education and Research (BMBF) is thanked for funding this German project under the Grant 03G0753A. The continuous support of K. Erbas (Potsdam) as project coordinator is highly appreciated. Our thanks go to I. Pieper for the ICP water analyses at the TU Berlin; H. Meyer (Potsdam) for stable-isotope measurements on the water samples, and R. Naumann (Potsdam) and F. Finger (Salzburg) for XRF measurements. O. Appelt and I. Schäpan (Potsdam) are acknowledged for their support with the electron microprobe and SEM, respectively. A. Förster (Potsdam) and P. Möller (Potsdam) provided many suggestions that helped improving the manuscript. The authors would like to thank the anonymous reviewers for their interesting and important suggestions and comments. A major acknowledgement goes to the Agency for Oil and Mineral resources in Surabaya East Java province (DINAS-ESDM).

**Competing interests**

The authors declare that they have no competing interests.

Received: 19 May 2015 Accepted: 1 October 2015
Published online: 26 October 2015

**References**

Belsky A, Hellenbrandt M, Karen VL, Luksch P. Acta Cryst. 2002;B58:364–9.

Bergerhoff G, Brown ID. Crystallographic databases—international union of crystallography. 1987.

Bogie I, Lawless JV, Rychagov S, Belousov V. Magmatic-related hydrothermal systems: classification of the types of geothermal systems and their ore mineralization. In: Proceedings of Geoconference in Russia, Kuril, 2005.

Brehme M, Moeck I, Kamah Y, Zimmermann G, Sauter M. A hydrotectonic model of a geothermal reservoir—a study in Lahendong, Indonesia. Geothermics. 2014;51:228–39.

Brehme M. The role of fault zones on structure, operation and prospects of geothermal reservoirs—a case study in Lahendong, Indonesia. Dissertation, University of Göttingen, 2015, p. 101.

Brehme M, Deon F, Haase C, Wiegand B, Kamah Y, Sauter M, Regenspurg S. Geochemical properties controlled by fault permeability in the Lahendong geothermal reservoir. Grundwasser. 2015 submitted.
Carn SA. Application of synthetic aperture radar (SAR) imagery to volcano mapping in the humid tropics: a case study in East Java, Indonesia. Bull Volcanol. 1999;61:92–105.
Carn SA. The Lamongan volcanic field, East Java, Indonesia: physical volcanology, historic activity and hazards. J Volcanol Geoth Res. 2000;95:81–108.
Carn SA, Pyle DM. Petrology and Geochemistry of the Lamongan Volcanic Field, East Java, Indonesia: primitive Sunda Arc Magmas in an extensional Tectonic Setting? J Petrol. 2001;4:1643–83.
Chaussard E, Amelung F. Precursory inflation of shallow magma reservoirs at west Sunda volcanoes detected by InSAR. Geophys Res Lett. 2012;39:L2131.
Deon F, Moeck I, Scheytt T, Jaya MS. Preliminary assessment of the geothermal system of the Tiris volcanic area, East Java, Indonesia. In: 74th EAGE conference and exhibition, Copenhagen, Denmark, 2012.
Deon F, Moeck IB, Jaya MS, Scheytt T, Putriatni DJ. Greenfield exploration of hidden geothermal magmatic systems by fluid chemistry—case study Lamongan East Java. In: 75th EAGE conference and exhibition, London, United Kingdom, 2013.
Fisher RV, Waters AC. Basesurge bed forms in maar volcanoes. Am J Sci. 1970;268:157–80.
Fournier RO. Lectures on geochemical interpretation of hydrothermal waters. UNU Geothermal Training Programme, 1989.
Giggenbach WF, Goguel RL. Collection and analysis of geothermal and volcanic waters and gas discharges. DSIR Report CD 2401, 4th edition, Pertone, New Zealand, 1989.
Hamilton W. Tectonics of the Indonesian regions. US Geological Survey Professional Paper 1078, 1979.
Heiken G. Tuff rings: examples from the Fort Rock-Christmas Lake Valley, south-central Oregon. J Geophys Res. 1971;76:5615–26.
Hochstein MP. Assessment and modeling of geothermal reservoirs (small utilizations schemes). Geothermics. 1988;17:15–49.
Hochstein MP, Browne PRL. Surface manifestations of geothermal systems with volcanic heat sources. In: Sigurdsson H, editor. Encyclopedia of volcanoes. New York: Academic; 2000. p. 835–55.
Hochstein MP, Sudarman S. History of geothermal exploration in Indonesia from 1970 to 2000. Geothermics. 2008;37:220–66.
Katili JA. Volcanism and plate tectonics in the Indonesian island arcs. Tectonophysics. 1975;26:165–88.
Kim Y, Lee KS, Koh D, Lee D, Lee S, Park W, Koh G, Woo N. Hydrogeochemical and isotopic evidence of groundwater salinization in a coastal aquifer: a case study in Jeju volcanic island, Korea. J Hydrol 2003;270:282–94.
Larson AC, Von Dreele RB. General structure analysis system (GSAS), Los Alamos National Laboratory Report LAUR, 2000, p. 86–748.
Lawless JV, White PJ, Bogie I. Tectonics features of Sumatra and New Zealand in relation to active and fossil hydrothermal systems: a comparison. In: Proceedings of the PANCRIM Congress 1995 Auckland New Zealand 12–22 November 1995, p. 311–316.
Le Bas MJ, Le Maitre RW, Streckeisen A, Zanettin B. A chemical classification of volcanic rocks based on the total alkali-silica diagram. J Petrol. 1986;27:745–50.
Marini L. Geochemical techniques for the exploration and exploitation of geothermal energy. Italy: University of Genua; 2000.
Moore JG, Nakamura K, Alcaraz A. The 1965 eruption of Taal volcano. Science. 1966;151:955–60.
Nicholson K. Geothermal fluids—chemistry and exploration techniques. Berlin: Springer; 1993.
Puspito NT, Shimazaki K. Mantle structure and seismo-tectonics of the Sunda and Banda arcs. Tectonophysics. 1995;251:215–28.
Rangin C, Jolivet L, Pubellier M, Azéma J, Briais A, Chotin P, Fontaine H, Huchon P, Maury R, Müller C, Rampnoux JP, Stephan JF, Tourmon J. A simple model for tectonic evolution of southeast Asia and Indonesia region for the past 43 m.y. Bulletin de la Société Géologique de France. 1990;8:275–89.
Rybach L, Muffler LJP. Geothermal systems: principles and case histories. New York: Wiley; 1981.
Simkin T, Siebert L. Volcanoes of the World. 2nd ed. Tucson: Geoscience Press; 1994. p. 349.
Sisson TW, Bronto S. Evidence for pressure release beneath magmatic arcs from basalt at Galunggu, Indonesia. Nature 1998;391:883–6.
Smyth RH, Hall R, Nichols GJ. Cenozoic volcanic arc history of East Java, Indonesia: the stratigraphic record of eruptions on an active continental margin. Geol Soc Am Spec Pap. 2008;436:199–222.
Sporrer P. Vergleichende ökologische Untersuchungen an Seen und Flüssen Indonesiens (Java und Süd Sumatra). Ph.D. Thesis, University of Giessen, Giessen, 1995, p. 1–247.
Toby BH. EXPGUI, a graphical user interface for GSAS. J Appl Crystallogr. 2001;34:210–3.
Whitford DJ, Nicholls IA, Taylor SR. Spatial variations in the geochemistry of quaterary lavas across the Sunda Arc in Java and Bali. Contrib Miner Petrol. 1979;70:341–56.